JMEPEG (2005) 14:10-17
DOI: 10.1361/10599490522310

1059-9495/$19.00

Characterization of Aluminum/Steel Lap Joint by Friction Stir Welding

A. Elrefaey, M. Gouda, M. Takahashi, and K. Ikeuchi

(Submitted March 11, 2004)

The welding of a lap joint of a commercially pure aluminum plate to a low carbon steel plate (i.e., Al plate top, and steel plate bottom) was produced by friction stir welding using various rotations and traveling speeds of the tool to investigate the effects of the welding parameters on the joint strength. The joint strength depended strongly on the depth of the pin tip relative to the steel surface; when the pin depth did not reach the steel surface, the joint failed under low applied loads. Meanwhile, slight penetration of the pin tip to the steel surface significantly increased the joint strength. The joint strength tended to increase with rotation speed and slightly decrease with the increase in the traveling speed, although the results were quite scattered. The effects of the welding parameters were discussed metallographically based on observations with optical and scanning electron microscopes.

Keywords aluminum, friction stir welding, lap joint, steel

1. Introduction

In friction stir welding (FSW), a rotating tool with a cylindrical shoulder is pushed into the material at the join line. The tool is then moved along this line, frictionally heating the material to high temperatures, at which point it is easily plasticized and forced to flow around the tool. A weld forms behind the tool as the stirred material is consolidated.

Joining dissimilar metals by conventional fusion-welding methods is rather complicated and can be quite difficult, and, as a result, many investigations (Ref 1-4) have reported on the application of the solid-state bonding to form dissimilar-metal joints. Although FSW is also a solid-state joining procedure, only limited amounts of information have been published on its application to dissimilar-metal joining, except for combinations of different aluminum (Al) alloys (Ref 5-7).

Recently, a few studies have been published on the FSW of Al to steel in a butt joint (Ref 8, 9), but for Al-to-steel lap joints only a very few studies have been reported (Ref 10). The present article investigates the performance of FSW Al-to-steel (Al/Fe) lap joints and the phenomena occurring at the interface during the FSW process from a metallurgical point of view.

2. Experimental

A plate of commercially pure aluminum (A1100H24), 2.0 mm thick, was friction-stir-welded to a plate of low carbon (C) steel (SPCC), 1.2 mm thick. This is shown schematically in Fig. 1. The chemical compositions of the aluminum and the steel plates are listed in Tables 1 and 2, respectively. The rotation and travel speeds of the tool used are listed in Table 3. The depth of the pin tip from the upper surface of the Al plate was fixed at 2.0 and 2.1 mm (i.e., 0.0 and 0.1 mm from the surface of the steel plate).

The tool (SKD61 steel) was composed of a shank, a shoulder, and a pin, as shown in Fig. 2. The tool axis was tilted by 3° with respect to the vertical axis of the plate surface.

The FSW tool, fixed in the holder, was slowly pushed into the Al plate to the specified pin depth and then forcibly traversed along the joint until the end of the weld was reached. The welding tool was then retracted while the tool continued to turn.

A. Elrefaey, M. Gouda, M. Takahashi, and **K. Ikeuchi,** Joining and Welding Research Institute, Osaka University, 11-1 Mihogaoka Ibaraki, Osaka, 567-0047, Japan. Contact e-mail: elrefaey@jwri.osaka-u.ac.jp.

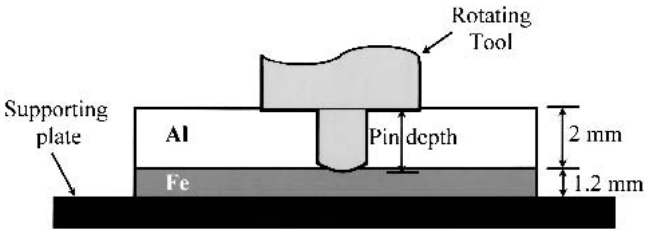

Fig. 1 Schematic illustration of the FSW of an aluminum plate to a steel plate

Table 1 Chemical composition of the commercially pure Al plate

Composition, mass%						
Si	**Fe**	**Cu**	**Mn**	**Mg**	**Ti**	**Al**
0.12	0.54	0.12	0.01	0.03	0.03	bal

Table 2 Chemical composition of the low C steel plate

Composition, mass%							
C	**Si**	**Mn**	**P**	**S**	**Al**	**N**	**Fe**
0.032	0.008	0.19	0.007	0.0156	0.043	0.0049	bal

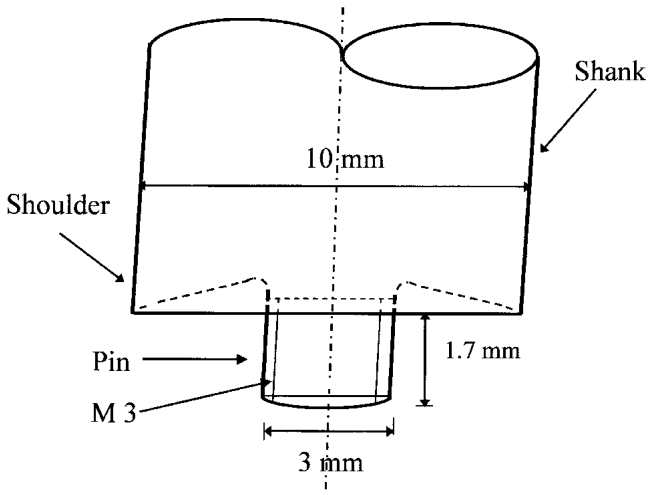

Fig. 2 Schematic illustration of the tool used for FSW

Table 3 Welding parameters and results from peel tests

Rotation speed, s^{-1}	Travel speed, mm/s	Pin depth, mm	Fracture load, N			Weld No.
16.7	3.3	2.1	171	175	190	1
	…	…	181	227	190	1′
	4.2	…	0	66	92	2
	…	…	94	194	6	2′
	5.0	…	0	0	91	3
	…	…	54	8	…	3′
25.0	3.3	2.1	66	468	556	4
	…	…	442	632	…	4′
	4.2	…	306	347	764	5
	…	…	…	284	236	5′
	5.0	…	598	629	813	6
	…	…	157	996	1010	6′
33.3	3.3	2.1	507	521	612	7
	…	…	…	615	759	7′
	4.2	…	396	466	493	8
	…	…	…	705	793	8′
	5.0	…	305	451	625	9
	…	…	595	504	…	9′
41.7	3.3	2.1	417	514	542	10
	…	…	…	701	…	10′
	4.2	…	83	549	598	11
	…	…	…	595	887	11′
	5.0	…	0	417	354	12
	…	…	189	1024	…	12′

The surfaces for the observations of microstructure were etched by 3% nital to reveal the steel microstructure and, subsequently, with a 1% hydrofluoric acid aqueous solution to reveal the aluminum microstructure. The microstructure was observed in the optical microscope, and in the scanning electron microscope (SEM) for closer observations.

A peel test was used to estimate the fracture load of the joints. The schematic view of the specimen used for the peel test is shown in Fig. 3.

Temperature measurements close to the Al/Fe interface (i.e., 0.3 mm from the upper surface of the steel plate) were carried out using a K-type thermocouple, percussion-welded to the bottom of drilled holes in the steel specimen. X-ray diffraction

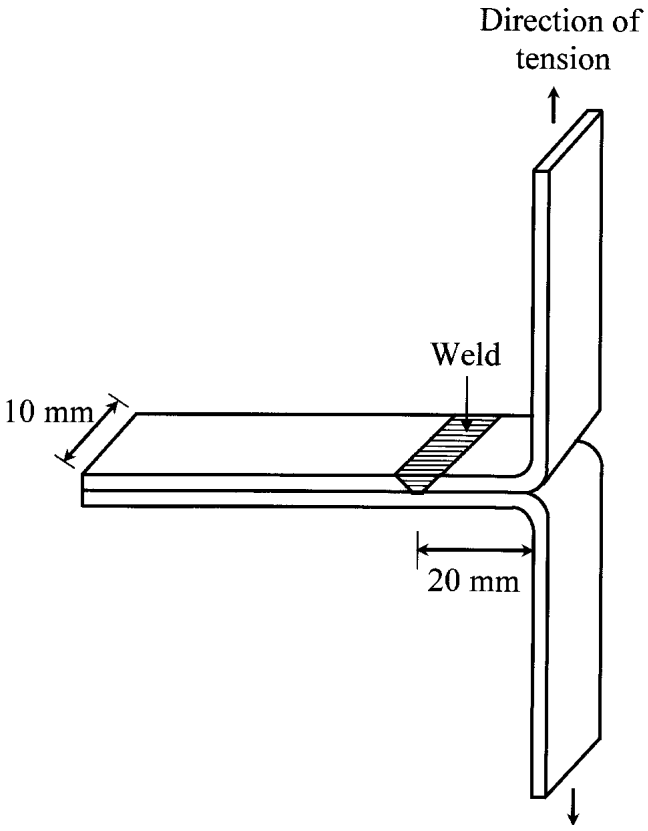

Fig. 3 Schematic view of the specimen for peel test

(XRD) analyses were carried out to identify the phases formed on the fractured surfaces of the joint after peel testing.

3. Experimental Results and Discussion

When the pin depth was 2.0 mm, the joints exhibited very low strength; most of them separated during the preparation of the specimen for the metallographic observation and the peel test.

Macrostructures of traverse sections of the joints are shown in Fig. 4. It should be noted that a change in the steel microstructure was observed in the area below the pin tip when the rotation speed was higher than 16.7 s^{-1}.

One of the main features of the aluminum macrostructure of the weld is that no clear "onion ring" structure, or thermomechanically affected zone, appeared in contrast to those reported in previous articles (Ref 11-13) on FSW of aluminum alloys.

The characteristic microstructures of the base metals and Al/Fe joints at a rotation speed of 41.7 s^{-1} are shown in Fig. 5 and 6, respectively. The microstructure of the base steel, as shown in Fig. 5(a), is ferritic due to its very low C content. The aluminum showed grains elongated in the rolling direction, as shown in Fig. 5(b). The microstructure of the aluminum of the joint, on the other hand, was characterized by equiaxed fine grains, as shown in Fig. 6(c) and (d). The grain size near the bond interface (area II) was coarser than that on the upper surface of the Al (area I) due to the effect of heat and strain generated in both areas. The area characterized by the equiaxed fine grain probably corresponds to the stirred zone. Between

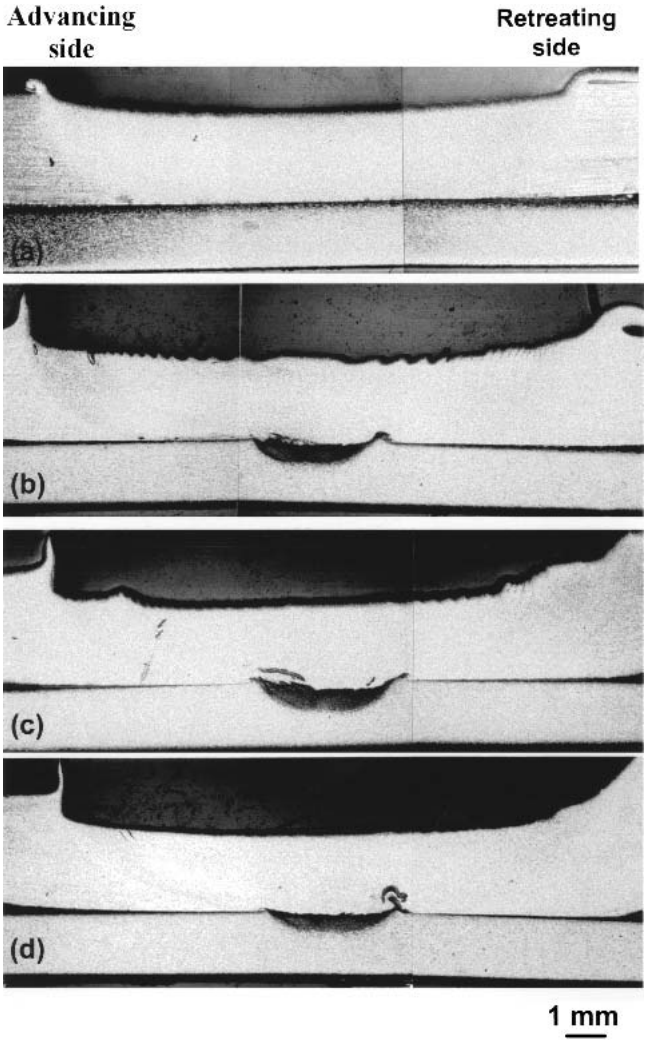

Fig. 4 Macrostructures of the transverse sections of joints. (a) Weld No. 1. (b) Weld No. 4. (c) Weld No. 7. (d) Weld No. 10

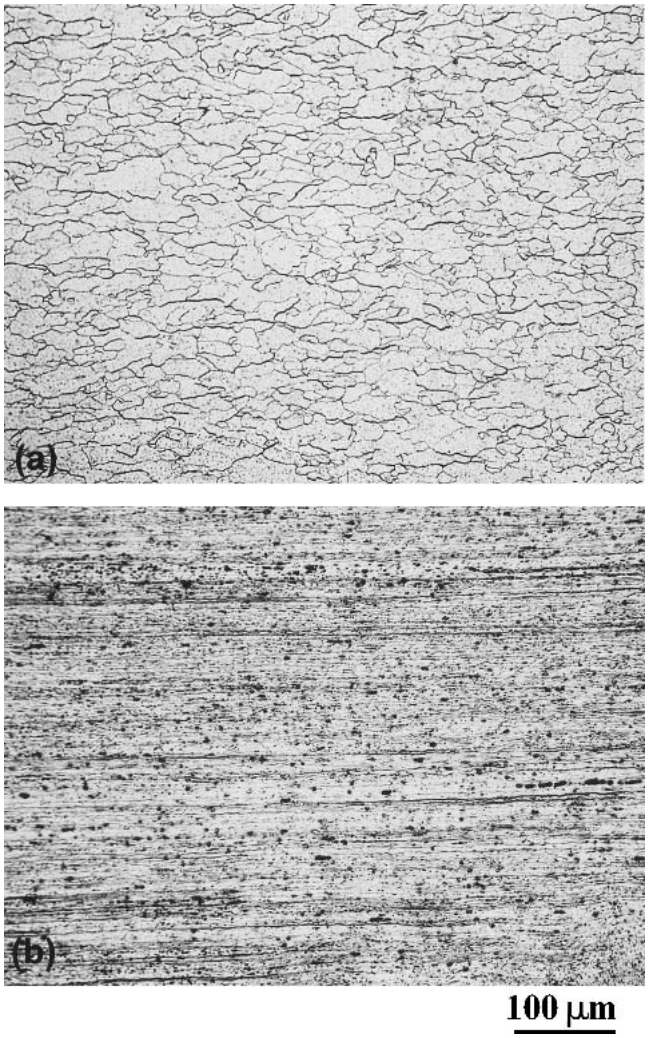

Fig. 5 Microstructures of the base metals of (a) steel and (b) aluminum plates

the area (I) and the base metal, narrow heat-affected-zones (areas IV and III) were observed, which were characterized by a coarse grain size, as shown in Fig. 6(b) and (e). Area V in the steel side was characterized by finer, more equiaxed grains than those in the base metal. This is shown in Fig. 6(f). In the transition zone between area V and the base steel (Fig. 6g), a coarser grain structure representing the steel HAZ was observed (area VI).

The very fine grain size in the steel close to the Al/Fe interface (area V) can be attributed to the recrystallization of the steel after undergoing heavy plastic deformation by the rotating pin, because the maximum temperature measured with thermocouples was not more than 793 K. The duration at these temperatures was not more than 3 s.

In the aluminum stirred zone near the weld interface, many Fe-rich particles were observed. This phenomenon is probably due to the stirring effect of the pin, which pulled small bits of steel from the surface and scattered them in the aluminum.

With an increase in the rotation speed, the grains of both aluminum and steel in all observed areas coarsened. This is probably due to the increased heat input. For example, the average grain size in the fine-grain zone of the steel at a rotation speed of 25.0 s^{-1} was approximately 3 μm, while it was 6 μm at a rotation speed of 41.7 s^{-1}. This result agrees with those of previous articles (Ref 14, 15). In contrast to rotation speed, increasing the travel speed decreased the heat input, which in turn decreased the grain size and decreased the steel fine grain zone area (Fig. 7).

SEM observations revealed that a layered structure formed in the steel fine-grain zone adjacent to the weld interface, as shown in Fig. 8. The Al content in the layered structure measured with EDX ranged from 5 to 20 at.%.

The distribution of hardness along the horizontal centerline of the Al plate is shown in Fig. 9. The hardness values on the aluminum side were almost constant in all directions. This is not surprising because the aluminum base metal is a non-heat-treatable, work-hardened aluminum alloy. The hardness distribution along the vertical axis to the weld interface is shown in Fig. 10. The average hardness in the fine-grain steel zone was 170 HV, while it was 116 HV in the base steel.

The highest values of hardness accompanied the layer structure at the Al/Fe interface, as shown in Fig. 11. (The average

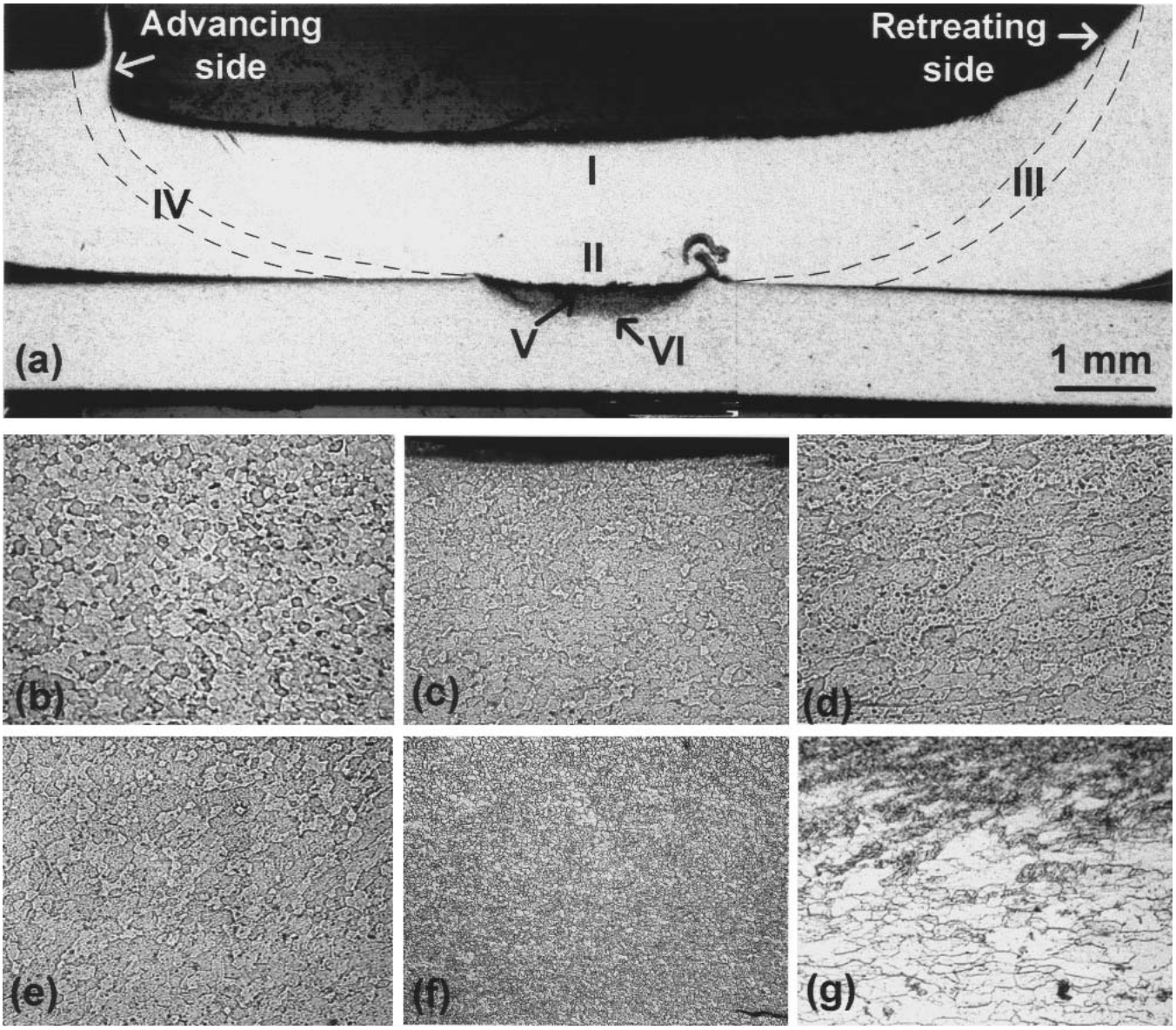

Fig. 6 Characteristic microstructures of different areas in Al/Fe FSW joint (Weld no. 10). (a) Macrostructure of the joint. (b) Al HAZ on the advancing side (area IV). (c) Fine equiaxed grain zone of aluminum (area I). (d) Fine equiaxed grain zone of aluminum (area II). (e) Al HAZ on the retreating side (area III). (f) Fine equiaxed grain zone of steel (area V). (g) Steel HAZ (area VI)

hardness in the layered structure was about 300 HV.) This is related to the formation of intermetallic compounds within this structure as suggested by XRD analyses of the fracture surfaces of the joints (Fig. 15).

The characteristic microstructure of the joint at the lowest rotation speed (16.7 s^{-1}) was similar to the microstructures at the higher rotation speeds (25.0-41.7 s^{-1}) except for the absence of the fine grain area and the layer structure in the steel side adjacent to the weld interface (Fig. 4).

The peel test fracture loads for the joints are shown in Table 3. All joints, except two, fractured at the weld line. Numbers 6 and 12 (with failure loads of 1026 and 1010 N, respectively) fractured near the weld interface. Although the measured values of the failure loads were scattered, they showed a general tendency to decrease slightly with increasing travel speed (i.e., 3.3-5 mm/s). Increasing the rotation speed of the tool from 16.7 to 25.0 s^{-1} improved joint strength, although a further increase from 25.0 to 41.7 s^{-1} caused only a slight change in the fracture load.

For most joints bonded at rotation speeds of 25.0 to 41.7 s^{-1}, fracture during the peel test occurred along the path shown in Fig. 12. Many Fe-rich fragments stuck to the fractured surface of the Al side. Closer observation of the circular area in Fig. 12(a) showed that the Fe-rich fragment consisted of a layered structure that was similar to those observed in Fig. 8. The results from a point analysis of the layered structure are listed in Table 4. The Fe and Al contents of the layered structure suggest the presence of intermetallic compounds. Thus, it can be considered that the fracture occurred mainly along the layer structure involving intermetallic compounds of the Al-Fe system.

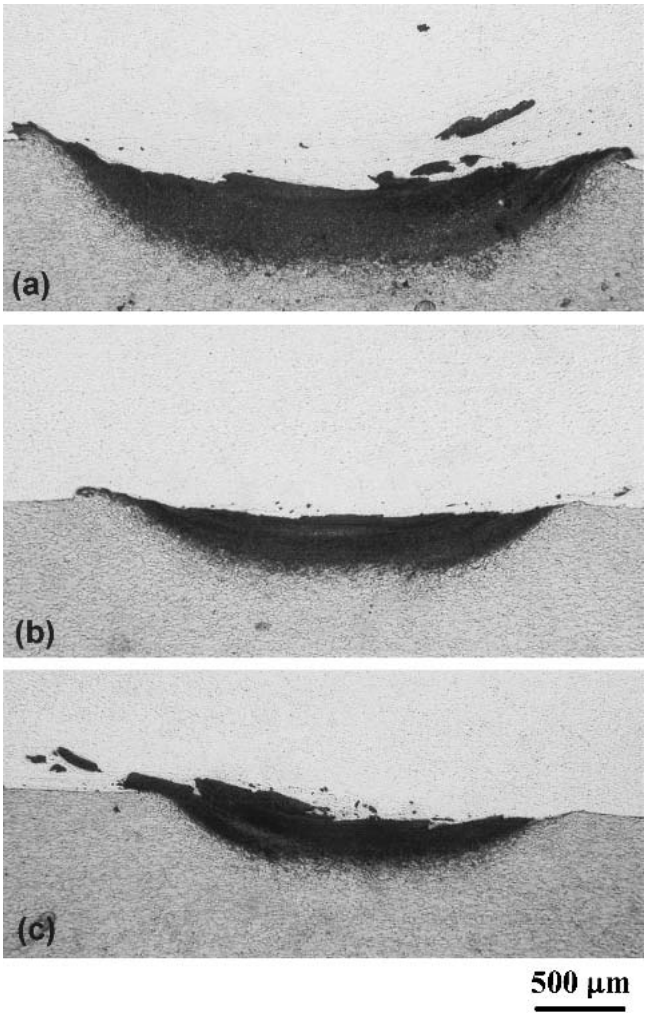

Fig. 7 The effect of travel speed on the size of the steel fine-grain zone. (a) Weld No. 10. (b) Weld No. 11. (c) Weld No. 12

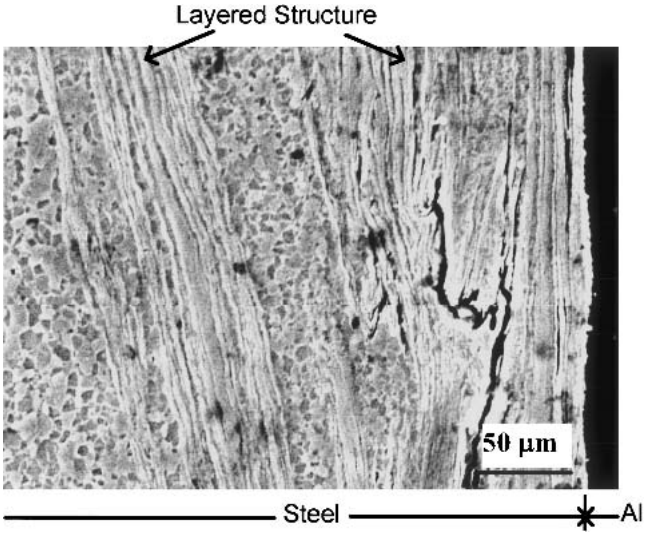

Fig. 8 Layered structure observed at the Al/Fe interface

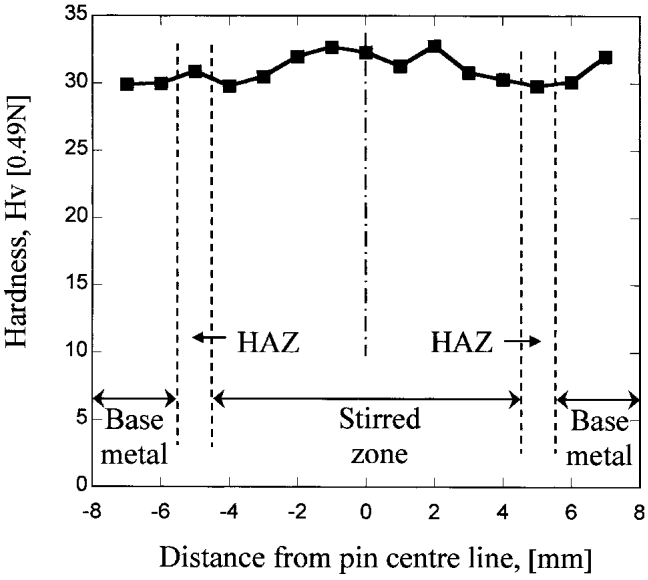

Fig. 9 Hardness distribution along the center line of the Al plate

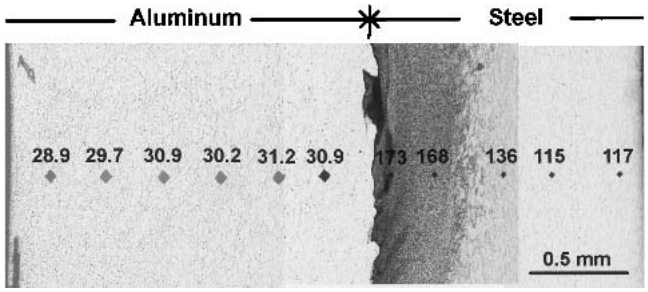

Fig. 10 Hardness distribution ($H_{0.49\ N}$) perpendicular to the Al/Fe interface (Weld No. 7)

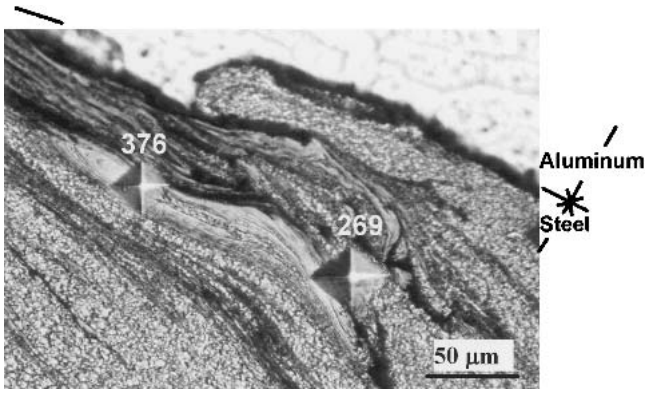

Fig. 11 Hardness values of the layered structure (Weld No. 7)

Table 4 Chemical analyses at points, 1 to 5, indicated in Fig. 12(c) (at.%)

	Points				
Elements	**1**	**2**	**3**	**4**	**5**
Fe	1	82	73	75	57
Al	99	18	23	25	43

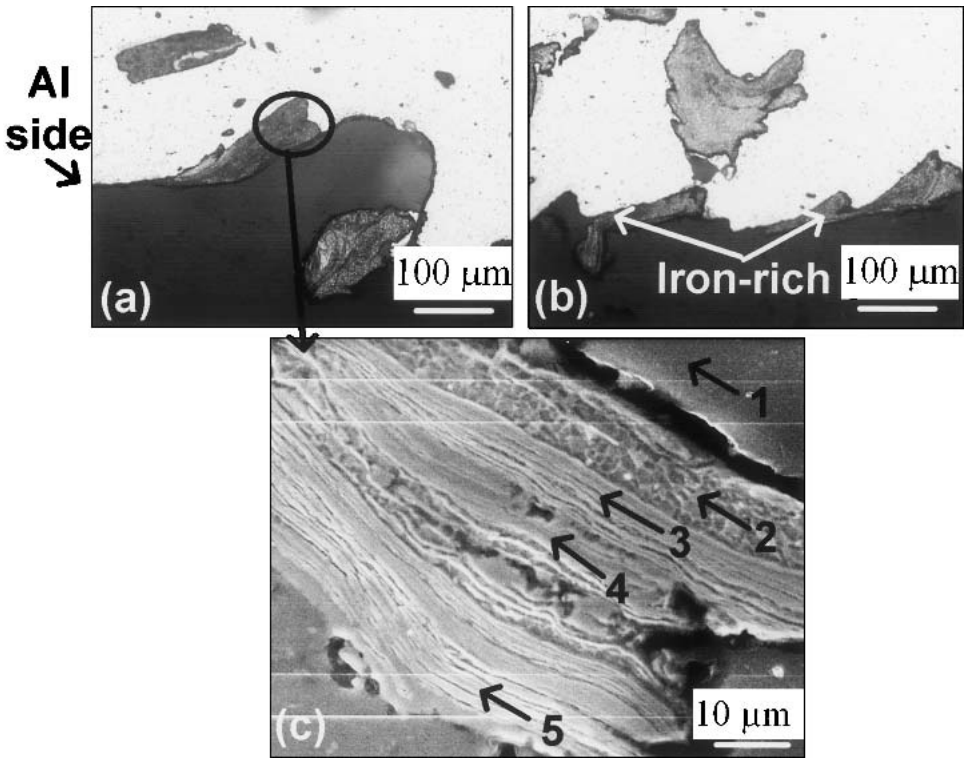

Fig. 12 Cross section of a fracture surface of the aluminum side (Weld No. 7). (a) and (b) Fe-rich fragment on the fractured surface. (c) Closer view of the circular area in (a)

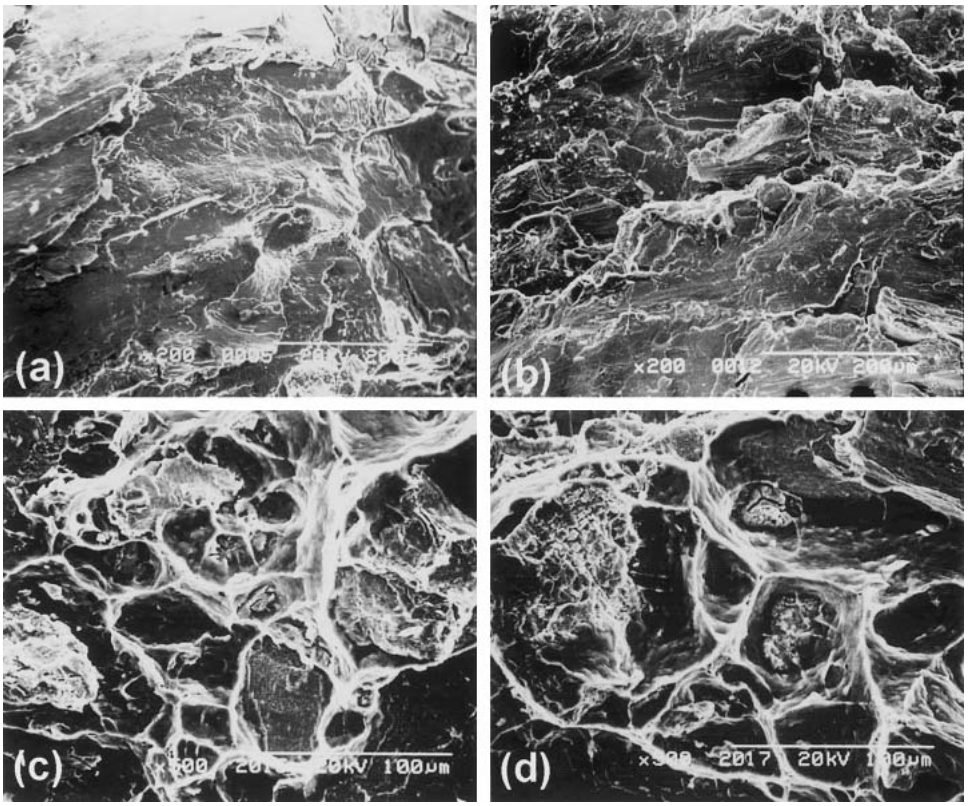

Fig. 13 Fracture surfaces of joint after the peel test (Weld No. 7). (a) Brittle morphology on the aluminum side. (b) Brittle morphology on the steel side. (c) Ductile morphology on the aluminum side. (d) Ductile morphology on the steel side

SEM micrographs of the fracture surfaces corresponding to the crack path shown in Fig. 12 are shown in Fig. 13. The fracture surfaces consisted mainly of two types of morphologies: brittle fracture, which was more prominent, and ductile fracture, which involved phases broken in a brittle manner. These two types of morphologies are shown in Fig. 13.

In contrast to these joints (i.e., a 16.7 s^{-1} rotation speed), aluminum and steel fracture surfaces were rather flat except for tear ridges of aluminum in very narrow areas, as shown in Fig. 14.

To identify the intermetallic compounds formed in the layered structure of the joint (e.g., rotation speeds of 25.0-41.7 s^{-1}), XRD patterns from the fractured surfaces were analyzed (Fig. 15a, b). As can be seen, intermetallic compounds of Al_5Fe_2 and $Al_{13}Fe_4$ were detected from both the aluminum and steel sides. This suggests that these intermetallic compounds

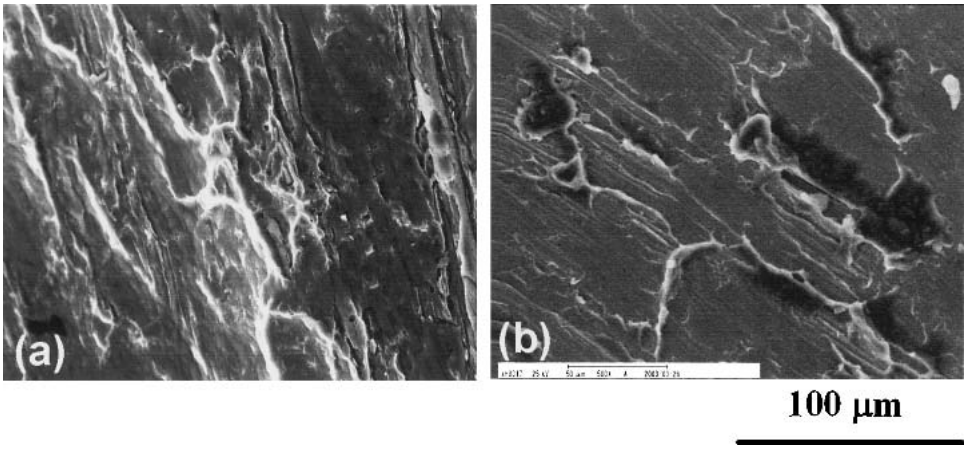

Fig. 14 Fracture surface of the (a) aluminum side and (b) steel side for joints welded at a rotation speed of 16.7 s^{-1}

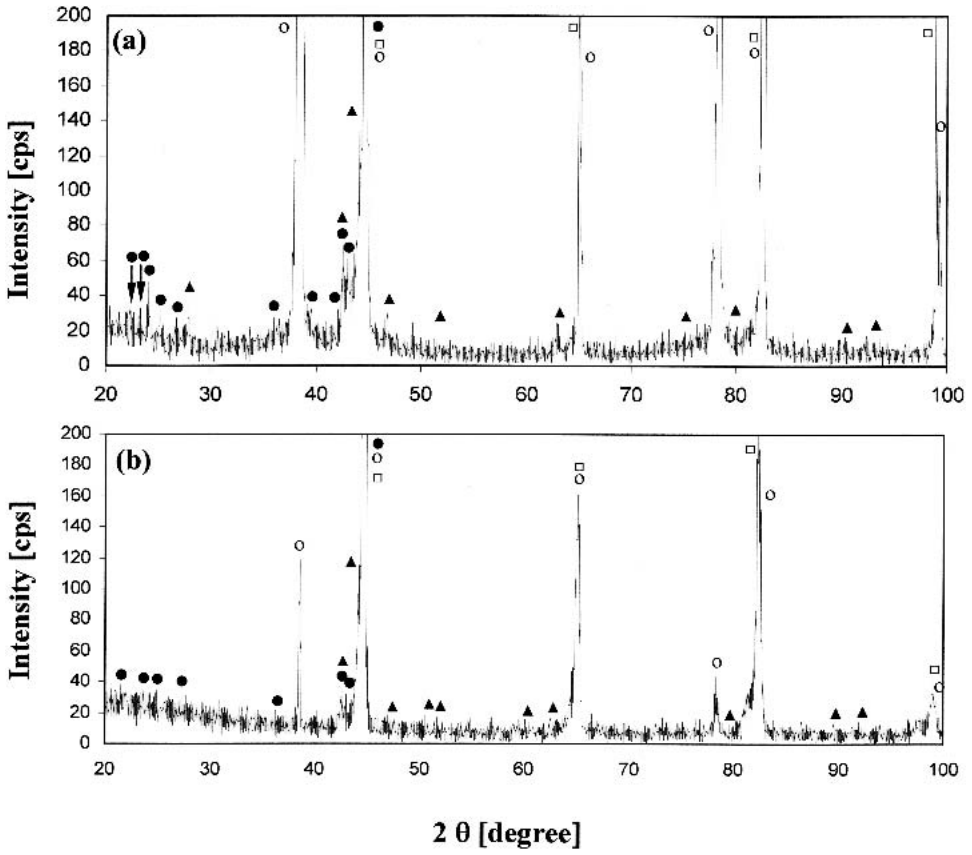

Fig. 15 XRD patterns from fracture surfaces of the (a) aluminum and (b) steel sides (Weld No. 10), where diffraction lines from Al, Fe, Al_5Fe_2, and $Al_{13}Fe_4$ were indicated by ○, □, ▲, and ●, respectively

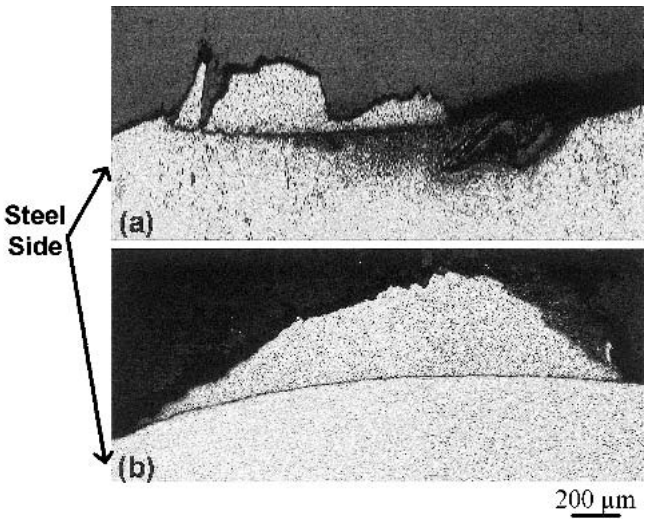

Fig. 16 Cross sections of fracture surfaces of the steel side for the specimens showing high fracture loads. (a) Weld No. 12. (b) Weld No. 6

were formed in the layered structure (Fig. 8) and are responsible for the brittle fracture (Fig. 13).

As shown in Table 3, two test specimens cut from Weld No. 6 and Weld No. 12 showed exceptionally high strength compared with the others bonded under the same conditions. The cross sections of the fracture surfaces of these specimens are shown in Fig. 16. There is no layered structure on the steel side of these specimens, and fracture occurred mainly in the Al, supporting the conclusion that the intermetallic compounds formed in the layered structure were responsible for the brittle fracture of the joints at lower loads.

These results suggest that it is possible to achieve quality joints between Al and steel using FSW by carefully controlling the pin depth to avoid the formation of an intermetallic-rich layered structure.

4. Conclusions

- A lap joint of a commercially pure aluminum plate to a low C steel plate was successfully welded by the FSW process.
- A slight difference in pin depth (0.1 mm) has a significant effect on the performance of the lap joints.
- The aluminum side of the joint showed an equiaxed, fine-grain morphology, and a heat-affected zone at the retreating and advancing sides. Meanwhile, the steel just under the rotating pin showed a very fine grain size that involved a layered structure in the area very close to the weld interface.
- By increasing the rotation speed and decreasing the travel speed, grains of both aluminum and steel in all characteristic areas were coarsened.
- The joints formed at rotation speeds between 25.0 and 41.7 s^{-1} had higher strength than those formed at a rotation speed of 16.7 s^{-1}.
- Fracture of the joints formed at higher rotation speeds occurred mainly in the layered structure, probably owing to the formation of intermetallic compounds such as Al_5Fe_2 and $Al_{13}Fe_4$.

References

1. M. Ghosh, S. Chatterjee, and B. Mishra, The Effect of Intermetallics on the Strength Properties of Diffusion Bonds Formed Between Ti–5.5Al–2.4V and 304 Stainless Steel, *Mater. Sci. Eng.,* Vol A 363, 2003, p 268-274
2. U. Kamachi Mudali, B.M. Ananda Rao, K. Shanmugam, R. Natarajan, and B. Raj, Corrosion and Microstructural Aspects of Dissimilar Joints of Titanium and Type 304L Stainless Steel, *J. Nucl. Mater.,* Vol 321 (No. 1), 2003, p 40-48
3. L. D'Alvise, E. Massoni, and S. J. Walløe, Finite Element Modelling of the Inertia Friction Welding Process Between Dissimilar Materials, *J. Mater. Proc. Technol.,* Vol 125-126, 2002, p 387-391
4. M. Yamamoto, M. Takahashi, and K. Ikeuchi, Interfacial Layer in Friction-Bonded Joint of Low Carbon Steel to Al-Mg Alloy (5083) and Its Influence on Bond Strength, *Mater. Trans., JIM,* Vol 45, 2004, p 296-299
5. Y. Li, L.E. Murr, and J.C. McClure, Flow Visualization and Residual Microstructures Associated with the Friction-Stir Welding of 2024 Aluminum to 6061 Aluminum, *Mater. Sci. Eng.,* Vol A 271, 1999, p 213-223
6. W.-B. Lee, Y.-M. Yeon, and S.-B. Jung, The Joint Properties of Dissimilar Formed Al Alloys by Friction Stir Welding According to the Fixed Location of Materials, *Scr. Mater.,* Vol 49, 2003, p 423-428
7. L. Karlsson, E.-L. Berqvist, and H. Larsson, Application of Friction Stir Welding to Dissimilar Welding, *Weld. World,* Vol 46, 2002, p 10-14
8. W. Takehiko, Y. Atsushi, and T. Hirohumi, Bonding of Steel and Aluminum Alloy by Interfacial Active Adhesion Bonding Method: Interfacial Active Adhesion Bonding of Dissimilar Materials with a Rotating Needle, National Meeting of the Japanese Welding Society, Vol 71, Japanese Welding Society, 2002, p 446-447 (in Japanese)
9. M. Tsubaki, M. Fukumoto, and T. Yasui, Evaluation of Joining Property Between Steel and Aluminum by Friction Stirring, National Meeting of the Japanese Welding Society, Vol 72, Japanese Welding Society, 2003, p 30-31 (in Japanese)
10. K. Yoshikawa and T. Harano, "Numerically Controlled Friction Stir Welding in Layered Dissimilar Metal Materials of Aluminum and Steel," Proceedings of the Third Symposium on Friction Stir Welding (Kobe, Japan), The Welding Institute, Sept 2001
11. G. Oertelt, S.S. Babu, S.A. David, and E.A. Kenik, Effect of Thermal Cycling on Friction Stir Welds of 2195 Aluminum Alloy, *Weld. Res.,* Vol 3 (suppl.), 2001, p 71-79
12. W.D. Lockwood, B. Tomaz, and A.P. Reynolds, Mechanical Response of Friction Stir Welded AA 2024: Experiment and Modeling, *Mater. Sci. Eng.,* Vol A323, 2002, p 384-353
13. M. Guerra, C. Schmidt, J.C. McClure, L.E. Murr, and A.C. Nunes, Flow Patterns During Friction Stir Welding, *Mater. Charact.,* Vol 49, 2003, p 95-101
14. C.G. Rhodes, M.W. Mahoney, W.H. Bingel, and M. Calabrese, Fine-Grain Evolution in Friction-Stir Processed 7050 Aluminum, *Scr. Mater.,* Vol 48, 2003, p 1451-1455
15. W.B. Lee, Y.M. Yeon, and S.B. Jung, Joint Properties of Friction Stir Welded AZ31B-H24 Magnesium Alloy, *Mater. Sci. Technol.,* Vol 19, 2003, p 785-790